Optics Letters

Impact of curvature on the optimal configuration of flexible luminescent solar concentrators

Mark Portnoi, Christian Sol, Clemens Tummeltshammer, and Ioannis Papakonstantinou*

Department of Electronic and Electrical Engineering, University College London, London WC1E 7JE, UK
**Corresponding author: i.papakonstantinou@ucl.ac.uk*

Received 21 March 2017; accepted 26 May 2017; posted 5 June 2017 (Doc. ID 290975); published 6 July 2017

Flexible luminescent solar concentrators (LSCs) could deliver integrated photovoltaics in all aspects of our lives, from architecture to wearable electronics. We present and experimentally verify a model for the optimization of the external optical efficiency of LSCs under varying degrees of curvature. We demonstrate differences between the optimization of flat and bent LSCs, showing that optimal fluorophore concentrations can differ by a factor of two.

OCIS codes: (160.2540) Fluorescent and luminescent materials; (220.1770) Concentrators; (230.7405) Wavelength conversion devices; (250.5460) Polymer waveguides; (260.6970) Total internal reflection; (350.6050) Solar energy.

https://doi.org/10.1364/OL.42.002695

Photovoltaic devices have the potential to be integrated into our lives on many scales, from large sizes such as building-integrated photovoltaics (BIPV) and vehicles, to smaller devices such as watch straps or furniture. One potential means of achieving this is luminescent solar concentrators (LSCs).

LSCs are transparent host matrices doped with fluorescent materials and were first invented in the 1970s [1,2]. The materials, or fluorophores, are typically fluorescent dyes [3–6], quantum dots [7–11], or rare-earth materials [12]. The fluorophores absorb light incident onto the device, before re-emitting at longer wavelengths. Re-emitted light is trapped within the host matrices by means of total internal reflection, allowing for concentration of light from larger to smaller areas on the edges. These edge surfaces are then coupled to photovoltaic panels, which convert the light into electrical energy. LSCs have been studied due to their high theoretical limits [13–15].

Typically host matrices are rigid materials, such as glass or polymers such as polymethyl methacrylate (PMMA) [16–18] or polylaurel methacrylate (PLMA) [10], lending themselves to flat planar geometries. Recently, however, the use of flexible host matrices, such as silicones [19,20], ultra-thin geometries, as well as fiber geometries [21–23], has led to broader potential of curved, bent, and coiled arrangements [11,24]. Combined with the ability to select both device transparency levels and color when choosing fluorophores, as well as the ability to cast LSCs into various shaped molds, LSCs provide a great degree of design freedom. This opens up opportunities for integration, such as self-powered wearable technologies, garden furniture that charges electronic devices, and electricity-generating tents.

The performance of an LSC is subject to several loss mechanisms [25]. Due to the non-unity quantum yield of fluorophores, some light that is absorbed is not re-emitted. In the case of overlap between fluorophore absorption and emission spectra, the LSC is subject to further non-unity quantum yield losses due to re-absorption. Once re-emitted, photons can be trapped within the host matrix by means of total internal reflection. If light reaching the top and bottom of the host matrix falls within the escape-cone angle, it will escape, contributing to a significant proportion of LSC losses. In order to optimize the LSC's external optical efficiency (i.e., the proportion of incident photons that are successfully guided to the edges of the LSC), a balance must be reached between having high enough fluorophore concentrations to absorb significant amount of the incident spectrum, yet low enough to not cause significant re-absorption losses. Maximum device efficiencies are the product of the LSC internal optical efficiency and the effective quantum efficiency of solar cells coupled to them. Re-absorption losses are prevalent when the average length before a photon is absorbed is short relative to the path required for a photon to reach the edges of the LSC. Upscaling of LSCs, therefore, strongly increases the aforementioned losses and makes efficiencies more sensitive to changes in the photon path length.

In this Letter, we explore how this optimization is affected by curvature. We have developed an in house Monte-Carlo-method-based ray-tracing model, which we implemented to simulate the performance and losses of LSCs, and the effect of incrementally bending the LSC. This model is experimentally verified and then used to perform large-area optimization. We compare the optimal concentration-thickness configurations of external optical efficiency of an LSC when flat to that when bent to a semi-circular arc. To the best of our knowledge, we demonstrate for the first time that in order to attain the highest external optical efficiency, the optimal concentration

for a bent LSC differs from that of a flat LSC. This is caused by three factors: (i) an increase in re-absorption losses due to longer path lengths within the LSC, (ii) an increase in escape cone losses due to increased escape cone angles on the outer surface of the LSC, and (iii) a further increase of escape cone losses due to the additional re-absorption. In addition, we show a decrease in absorbed light due to higher reflections off the top surface at acute angles of incidence near the edges of the LSC, which is constant with respect to LSC thickness for fixed radii of curvature.

For the purpose of model verification we fabricated three flexible LSCs, following the methods described in [20]. Polydimethylsiloxane (PDMS) was used as the host matrix (Sylgard 184, Dow Corning) due to its optical transparency and flexibility. Pyrromethene 567 (Exciton) was chosen as a fluorophore, which has a peak absorption at 520 nm, a Stokes shift of 18 nm, and high quantum yield in PDMS (93%), measured in agreement with the literature [20]. This fluorophore is used for this Letter as proof of concept; however, a wide range of fluorophores may be used according to the desired design parameters. The LSC dimensions and fluorophore concentrations are listed in Table 1. In order to demonstrate the full validity of the model, we compare LSCs with varying dimensions and concentrations.

We characterized each LSC's performance following the methods and equipment described in [25], in which the flux escaping both the edges and the larger LSC faces can be measured. The LSCs are placed into an integrating sphere and excited with a monochromatic light, and changes in the spectral distribution are measured using a spectrophotometer. Such changes can be used to derive the various photon fates. The LSCs were excited with monochromatic light of fullwidth half-maximum (FWHM) 20 nm and central wavelength 480 nm, chosen such that the wavelength is in a high-absorption region of the fluorophore, without overlapping with the emission spectrum. To determine inputs for the simulation, (i) we measure the host matrix refractive index using an ellipsometer (Semilabs SE2000), (ii) the fluorophore absorption spectrum is measured using a UV-VIS spectrometer (Shimadzu), (iii) the emission spectrum is measured using a fluorescence spectrometer (Edinburgh Instruments), and (iv) the beam diameter is measured at the LSC as 13 mm, the shape of which is modeled with a Gaussian distribution of FWHM 10 mm.

For the verification of the flat LSC simulations, we separate the fates of photons absorbed inside the LSC. These photons can be categorized into three possible outcomes: photons lost due to non-unity quantum yields, escape-cone losses, and, finally, internal optical efficiency. Internal optical efficiency is the proportion of photons that, once absorbed, are successfully guided to the edges. To calculate the external optical efficiency, which incorporates reflections off the top surface and the absorbance of the fluorophore, all that is required is to multiply the internal optical efficiency by the proportion of incident photon that the LSC has absorbed [25]. Experimental results for each sample, with no curvature applied, show good agreement with simulations, as demonstrated in Fig. 1. Experimental values are the mean value from three measurements, and all measured internal optical efficiency values fall within a 4% relative agreement with the simulated values.

Table 1. Dimensions and Concentrations of Sample LSCs

LSC Sample #	Dimensions (mm)	Concentration (M)
1	50 × 50 × 4	5×10^{-5}
2	100 × 100 × 4	1×10^{-4}
3	100 × 100 × 4	5×10^{-6}

We now extend the model to include curvature, modeling the LSCs bent onto arc shapes of decreasing radii of curvatures. We investigate the effect of the tightening curvature on the internal optical efficiency. For the purpose of model verification, we used Sample 3 from Table 1, as it has the highest internal optical efficiency of the three, so a more significant change is expected when curvature is applied.

Increasing levels of curvature are applied to the LSC within the integrating sphere using transparent tape, as shown in Fig. 2(a). These levels of curvature correspond to 1/R (R) values, in m^{-1}(m), of: 0 (flat), 15.9 (0.063), 21.3 (0.047), and 27.0 (0.037). Efficiency measurements are taken using the same methods as used for the flat LSCs. Experimental results are in agreement with simulations, which show a drop of internal optical efficiency from 0.495 when flat to 0.488 at a 1/R of 27, as shown in Fig. 2(b). Error bars show the range of three measurements for each applied curvature, while the crosses show the mean values, which agree with simulation (blue line) to within 2% in relative terms.

While the method shows good agreement with the simulation, the variance in experimental measurement is high, relative to the change in internal optical efficiency. This variance can be partly attributed to variation in LSC position within the integrating

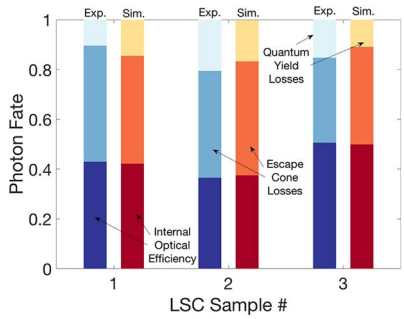

Fig. 1. Experimental (blue) and simulated (red) performance of the three different flat LSCs. The photon fate is shown for each sample; quantum yield losses (top), escape cone losses (middle), and internal optical efficiency (lowest).

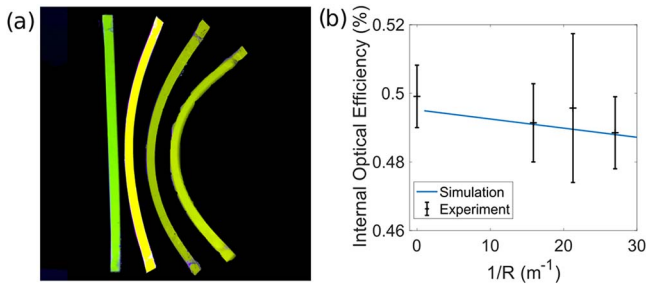

Fig. 2. (a) Superimposed images of LSC sample 3 under UV illumination, with four levels of curvature applied. (b) Simulated (line) and experimental (bar plots) performance of LSC sample 3. The 1/R values measured correspond to the curvatures shown in (a).

sphere between measurements. The flexible nature of the LSCs means that the curvature may not be consistent throughout the LSC, and between measurements. Any changes in the position of the LSC relative to the excitation beam can increase the variation, as internal optical efficiency is dependent on which part of the LSC is illuminated. As LSC sizes increase, the internal optical efficiency becomes less dependent on illumination position, and so variation is decreased.

We use our model to investigate the optimization of large-scale flexible LSCs. We look to optimize the external optical efficiency, which, in addition to internal optical efficiency, incorporates collecting surface reflections and fluorophore absorbance. We simulate an LSC with a 1 m × 1 m collecting surface. Two radii of curvature are modeled—one flat, and one such that the LSC is bent to a semi-circle, i.e., the radius of curvature is equal to l/π, where l is the length of the LSC (1m, in this case.) A graphical representation of these arrangements is shown in Fig. 3. The AM1.5G solar spectrum is used in order to simulate conditions as close to real world as possible. While not necessarily the best-performing fluorophore for LSCs, for continuity and as proof of concept, we continue to use Pyrromethene-567 as our fluorophore. Within our simulations we find, for a range of thicknesses between 0.01 cm and 1 cm, a set of optimum concentration values. In this case, the optimum concentration-thickness pairing is defined by one that yields the highest external optical efficiency.

Figure 4 shows the simulation results for a whole-width beam illumination of both a flat (top) and curved (bottom) LSC. For each thickness, there is an optimum concentration, at which the concentration is high enough to absorb a significant proportion of the solar spectrum, while low enough to avoid significant losses due to re-absorption. As LSC thickness is increased, concentrations for optimum LSC external efficiencies decrease due to increased optical path lengths to the edges of the LSC.

By plotting a line joining the optimal thickness-concentration pairings, we can observe that the optimal pairings are affected by curvature. Our simulations show, as evident in Fig. 4, that the gradient of this line is steeper for the flat LSC ($m = -0.3520$, where m is the gradient of the locus) than for the LSC bent to a semi-circular shape ($m = -0.2319$). At large thicknesses, such as 1 cm, the optimum concentration for both flat and bent are approximately $10^{-4.5}$ M at 1 cm. At this concentration, the external optical efficiencies are 10.18% and 10.12%, respectively, differing by less than 1%. As the thickness decreases, however, the optimum concentrations diverge. At 0.01 cm, for example, the optimum concentration for the flat LSC is $10^{-3.808}$ M, while for the bent LSC, it is $10^{-4.077}$ M. This amounts to almost half as many fluorophores used to reach optimum concentration for the bent LSC than the flat. This can be explained by a change in the path length for a photon to reach the edge of an LSC when the LSC is bent. At this thickness, the optimal external optical efficiencies are 0.27% and 0.25% for flat and bent, respectively, differing by 8%. If the optimum concentration for flat LSCs was used for both cases, the bent configuration would show an optical efficiency of only 0.22%. While the enhancement due to the change in optimization in absolute terms of 0.03% is small, this represents a relative enhancement of 14%. The use of more

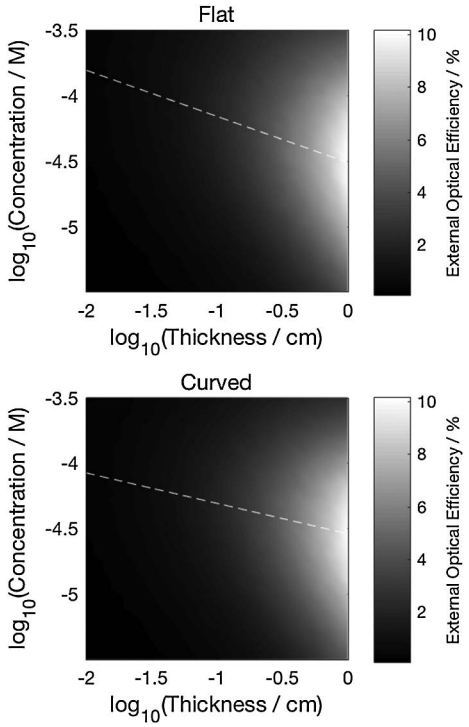

Fig. 4. Simulated external optical efficiencies of 1 m × 1 m LSCs for a range of thicknesses and concentrations. The simulation was run for flat (top) and curved (bottom). The dashed lines show the loci of optimum concentration-thickness pairings.

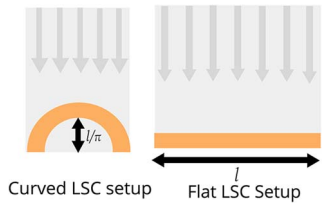

Fig. 3. Graphic representing the two grades of curvature. The beam width is simulated between such that all of the LSC collecting surface is illuminated with a flat intensity profile. The LSC setup is bent to a radius of curvature of l/π (left) and flat (right), where l is the length of the LSC.

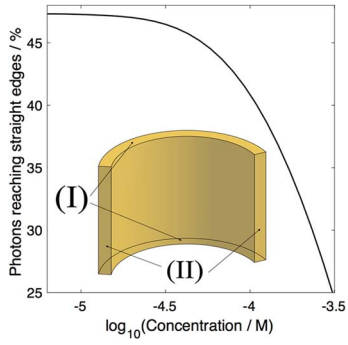

Fig. 5. Simulated share of waveguided light that reaches the straight edges (II) of the LSC plotted against concentration for a 1 m × 1 m × 0.01 m curved LSC. Inlet graphic showing the curved (I) and straight (II) edges of the LSC.

efficient luminophores would result in a larger absolute enhancement.

Bending an LSC results in a less direct path from the interior of the LSC to the edges (there is no direct line-of-sight path for photons to reach the edges), with additional induced reflections. Larger path lengths result in increased re-absorption losses, in turn lowering the optimum concentration of the LSC. This effect is more dominant for thin LSCs, due to the higher optimum concentrations. At higher concentrations, the attenuation length is shorter. Any increase in optical path length towards the edge of the LSC will be larger relative to attenuation. The difference between the two optimal configuration loci therefore increases as thickness decreases.

To demonstrate the effect of a longer path length to the edge of the LSC, we model the proportion of photons reaching the curved edges of the LSC (I in Fig. 5) relative to the share of photons that reach the straight edges of the LSC (II in Fig. 5). We vary the concentration, thus varying the photon attenuation length. Photons that reach the straight edges have traveled a longer distance due to the applied curvature. As shown in Fig. 5, at low concentrations, successfully guided photons reach all edges equally. As concentration increases, the attenuation length is decreased, thus re-absorption is increased. Due to increased re-absorption, the percentage of photons that reach the straight edges is decreased: most successfully guided photons travel along the flat plane of the LSC.

Another impact on the external optical efficiency of the LSC when bent is additional reflection off the collecting surface of the LSC. When the LSC is flat, illumination from perpendicular to the surface has an approximately 3% chance of reflection (for air to PDMS interface). As the LSC is bent, a proportion of the collecting surface is turned to an acute angle relative to the illuminating source. As the angle of incidence becomes more acute, the chance of reflection is increased; 10% at 65 deg incidence, and over 50% from above 85 deg incidence. In the case of the 1 m × 1 m LSC, this amounts to an increase in total collecting surface reflections of incident sunlight from 3% to 5% at a radius of curvature of l/π. While collecting surface reflections result in a lower external optical efficiency over all concentration-thickness pairings for a single illumination angle, this can result in LSCs being less dependent on the incident source angle, enhancing their ability to collect sunlight at varied angles of incidence [24]. This effect is independent of device thickness and concentration and does not affect the optimization of these parameters.

In conclusion, we have demonstrated and verified a model for the optimization of flexible LSCs, both flat and at varied degrees of curvature. We have shown that the fluorophore concentration optimization of curved LSCs diverges from that of flat LSCs. This effect is exaggerated as the device thickness is decreased. By modeling which LSC edges photons reach, we make evident that this effect is due to the longer path length for photons induced by curvature. An increase in the optical path length of light inside the LSC compared to that of the absorption length must be countered by a lower fluorophore concentration. This can be overcome by reducing re-absorption by means of novel fluorophores with high quantum yields and low spectral overlap, fluorophore alignment [26–28], or by combining fluorophores by means of Forster energy transfer [28–30]. We expose that additional consideration is required when designing and integrating curved or flexible LSCs into devices.

Funding. Engineering and Physical Sciences Research Council (EPSRC) Doctoral Training Award; H2020 European Research Council (ERC) Starting Grant "Intelglazing" (679891); University College London (UCL).

REFERENCES

1. W. H. Weber and J. Lambe, Appl. Opt. **15**, 2299 (1976).
2. A. Goetzberger and W. Greubel, Appl. Phys. **14**, 123 (1977).
3. A. Mirloup, P. Retailleau, and R. Ziessel, Tetrahedron Lett. **54**, 4456 (2013).
4. W. E. Benjamin, D. R. Veit, M. J. Perkins, E. Bain, K. Scharnhorst, S. Mcdowall, D. L. Patrick, and J. D. Gilbertson, Chem. Mater. **26**, 1291 (2014).
5. A. Sanguineti, M. Sassi, R. Turrisi, R. Ruffo, G. Vaccaro, F. Meinardi, and L. Beverina, Chem. Commun. **49**, 1618 (2013).
6. G. A. Reynolds and K. H. Drexhage, Opt. Commun. **13**, 222 (1975).
7. J. Bomm, A. Büchtemann, A. J. Chatten, R. Bose, D. J. Farrell, N. L. A. Chan, Y. Xiao, L. H. Slooff, T. Meyer, A. Meyer, W. G. J. H. M. Van Sark, and R. Koole, Solar Energy Mater. Sol. Cells **95**, 2087 (2011).
8. I. Coropceanu and M. G. Bawendi, Nano Lett. **14**, 4097 (2014).
9. C. Li, W. Chen, D. Wu, D. Quan, Z. Zhou, J. Hao, and J. Qin, Sci. Rep. **5**, 17777 (2015).
10. F. Meinardi, H. McDaniel, F. Carulli, A. Colombo, K. A. Velizhanin, N. S. Makarov, R. Simonutti, V. I. Klimov, and S. Brovelli, Nat. Nanotechnol. **10**, 878 (2015).
11. F. Meinardi, S. Ehrenberg, L. Dhamo, F. Carulli, M. Mauri, F. Bruni, R. Simonutti, U. Kortshagen, and S. Brovelli, Nat. Photonics **11**, 177 (2017).
12. C. Liu, R. Deng, Y. Gong, C. Zou, Y. Liu, X. Zhou, and B. Li, Int. J. Photoenergy **2014**, 1 (2014).
13. G. Smestad, H. Ries, R. Winston, and E. Yablonovitch, Sol. Energy Mater. **21**, 99 (1990).
14. I. Papakonstantinou and C. Tummeltshammer, Optica **2**, 841 (2015).
15. E. Yablonovitch, J. Opt. Soc. Am. **70**, 1362 (1980).
16. F. Meinardi, A. Colombo, K. A. Velizhanin, R. Simonutti, M. Lorenzon, L. Beverina, R. Viswanatha, V. I. Klimov, and S. Brovelli, Nat. Photonics **8**, 392 (2014).
17. S. M. El-Bashir, F. F. Al-Harbi, H. Elburaih, F. Al-Faifi, and I. S. Yahia, Renewable Energy **85**, 928 (2016).
18. R. Reisfeld, M. Eyal, V. Chernyak, and R. Zusman, Sol. Energy Mater. **17**, 439 (1988).
19. M. Buffa and M. G. Debije, Springer Ser. Mater. Sci. **190**, 247 (2014).
20. C. Tummeltshammer, A. Taylor, A. J. Kenyon, and I. Papakonstantinou, Opt. Lett. **41**, 713 (2016).
21. O. Y. Edelenbosch, M. Fisher, L. Patrignani, W. G. J. H. M. van Sark, and A. J. Chatten, Opt. Express **21**, A503 (2013).
22. S. F. H. Correia, P. P. Lima, P. S. André, M. R. S. Ferreira, and L. A. D. Carlos, Solar Energy Mater. Sol. Cells **138**, 51 (2015).
23. I. Parola, M. A. Illarramendi, J. Zubia, E. Arrospide, G. Durana, N. Guarrotxena, O. García, R. Evert, D. Zaremba, H.-H. Johannes, and F. Recart, "*Organic Photonic Materials and Devices XIX*" (2017), paper 101010Z.
24. B. Vishwanathan, A. Reinders, D. de Boer, L. Desmet, A. Ras, F. Zahn, and M. Debije, Solar Energy **112**, 120 (2015).
25. C. Tummeltshammer, A. Taylor, A. Kenyon, and I. Papakonstantinou, Solar Energy Mater. Sol. Cells **144**, 40 (2016).
26. M. G. Debije and P. P. C. Verbunt, in *Technical Proceedings of the NSTI Nanotechnology Conference and Expo* (NSTI-Nanotech, 2011), Vol. **1**, p. 584.
27. M. Fisher, D. Farrell, M. Zanella, A. Lupi, P. N. Stavrinou, and A. J. Chatten, Appl. Phys. Lett. **106**, 041110 (2015).
28. C. Tummeltshammer, A. Taylor, A. J. Kenyon, and I. Papakonstantinou, J. Appl. Phys. **116**, 173103 (2014).
29. C. Tummeltshammer, M. Portnoi, S. A. Mitchell, A.-T. Lee, A. J. Kenyon, A. B. Tabor, and I. Papakonstantinou, Nano Energy **32**, 263 (2017).
30. J. E. A. Webb, K. Chen, S. K. K. Prasad, J. P. Wojciechowski, A. Falber, P. Thordarson, and J. M. Hodgkiss, Phys. Chem. Chem. Phys. **18**, 1712 (2016).